NO_2 Adsorption on Ultrathin θ-Al_2O_3 Films: Formation of Nitrite and Nitrate Species

Emrah Ozensoy, Charles H. F. Peden, and János Szanyi*

Institute for Interfacial Catalysis, Pacific Northwest National Laboratory, P. O. Box 999, MSIN K8-93, Richland, Washington 99352

Received: April 20, 2005; In Final Form: June 7, 2005

Interaction of NO_2 with an ordered θ-Al_2O_3/NiAl(100) model catalyst surface was investigated using temperature programmed desorption (TPD) and X-ray photoelectron spectroscopy (XPS). The origin of the NO_x uptake of the catalytic support (i.e., Al_2O_3) in a NO_x storage catalyst is identified. Adsorbed NO_2 is converted to strongly bound nitrites and nitrates that are stable on the model catalyst surface at temperatures as high as 300 and 650 K, respectively. The results show that alumina is not completely inert and may stabilize some form of NO_x under certain catalytic conditions. The stability of the NO_x formed by exposing the θ-Al_2O_3 model catalyst to NO_2 adsorption increases in the order NO_2 (physisorbed or N_2O_4) < NO_2 (chemisorbed) < NO_2^- < NO_3^-.

1. Introduction

Metal oxide surfaces play a key role in numerous materials engineering processes, in semiconductor and sensor applications, as well as in heterogeneous catalytic systems.[1] Due to its high operational versatility and durability, Al_2O_3 has been widely used as catalyst support material for various important heterogeneous catalytic processes such as the selective catalytic reduction (SCR) of NO_x species originating from the combustion of fossil fuels.[2−4] Recently, Al_2O_3 surfaces have also been proposed to be an effective catalyst support for the after-treatment of lean-burn-engine emissions.[5−7] In this technology, the environmentally hazardous NO_x species, emitted by the lean-burn engines operated in alternating lean (abundant in O_2) and rich (abundant in hydrocarbons, CO, and H_2) conditions, are trapped and successively reduced to less hazardous N-containing compounds by a BaO and transition metal based NO_x storage system. In these NO_x storage traps, NO(g), which constitutes the major portion of the untreated NO_x emissions, is believed to be first oxidized catalytically to NO_2 on the transition metal sites (e.g., Pt or Rh) and then stored by the BaO sites as nitrates during the lean cycle. Subsequently, these trapped nitrate species are reduced on the transition metal sites during the rich cycle, regenerating the fresh BaO sites for the next catalytic cycle. Although BaO is the crucial component in these NO_x traps with a NO_x uptake that is significantly higher than that of the Al_2O_3 support, recent studies revealed that Al_2O_3 was not completely inert during NO_x adsorption.[8]

NO_2 is a radical that exhibits a rich chemistry on oxide surfaces, where it can act as a Lewis acid (electron acceptor) and/or a Lewis base (electron donor).[9] Depending on the morphology and the electronic nature of the oxide surface, NO_2 is known to either adsorb molecularly or react to form N, NO, N_2O, or NO_3 species.[10−19] It has also been reported that the relative NO_x uptakes of strongly ionic alkaline earth metal oxides are closely related to the strength of the Madelung potential of the corresponding crystals,[17] the extent of reducibility/oxidizability of the metal oxide surface,[9] and the surface defect density.[11−13]

Prior reports focusing on the fundamental aspects of the interaction between NO_2 and metal oxide surfaces includes studies using MgO,[9,12−14,18] ZnO,[15] BaO,[8,9,16−18,20−25] CaO,[9,18,26] SrO,[9,18] Al_2O_3,[8,10] CeO_2,[14] TiO_2,[11] Cr_2O_3,[12] $Fe_xN_yO_z$,[14,19] and CuO.[14]

Since, a molecular understanding of the interaction of NO_2 molecules and metal oxides, in particular Al_2O_3, is important for the design and improvement of NO_x storage systems, we investigated a model system: NO_2 on ordered θ-Al_2O_3 ultrathin films, the latter grown epitaxially on a NiAl(100) bimetallic substrate. Using temperature programmed desorption (TPD) and X-ray photoelectron spectroscopy (XPS) data, the formation and stability of different NO_x species are discussed.

2. Experimental Section

Experiments were performed in an ultrahigh vacuum (UHV) surface analysis chamber ($P_{base} \sim 3 \times 10^{-10}$ Torr) equipped with conventional surface spectroscopic probes, a high-pressure cell for IR experiments, and a Tectra ECR plasma source. The NiAl(100) single crystal used in the experiments (Princeton Scientific Corp., 10 mm diameter, 2 mm thick) was polished on both sides and spot-welded onto a U-shaped Ta wire. A C-type thermocouple was spot-welded to the top edge of the crystal for temperature measurements. Cleaning of the NiAl-(100) crystal was performed by alternating cycles of Ar^+ ion sputtering (V_{beam} = 1.5 kV, I_{beam} = 1.5 μA) and high-temperature UHV anneals at 1200 K. The cleanliness of the surface was checked with Auger electron spectroscopy (AES) and low energy electron diffraction (LEED). TPD experiments were performed using a differentially pumped UTI quadrupole mass spectrometer (QMS) by applying −70 V bias voltage on the spectrometer shield to constrain the ionizing electrons to the interior of the QMS shield, to prevent any possible electron beam damage on the sample. All of the TPD data presented in this study were obtained by ramping the temperature of the crystal at a constant rate of 2 K/s. A tubular pinhole doser, positioned in close proximity of the sample (∼2 mm away), was used in the adsorption experiments, which allowed the background pressure in the chamber to stay in the $\sim 10^{-10}$ Torr

* Corresponding author. E-mail: janos.szanyi@pnl.gov.

10.1021/jp052053e CCC: $30.25
Published on Web 08/04/2005

range during the dosing processes, to minimize background desorption artifacts in the TPD data.

Before the introduction of NO_2 gas to the vacuum chamber, the gas dosing line and the pinhole doser were passivated by flushing NO_2 gas through the dosing lines for an extended period of time. Passivation of the dosing line was also monitored with the QMS by following the 46 amu signal with respect to the 30 amu signal for a constant flux of NO_2. The saturation of the 46 amu/30 amu ratio indicated the deactivation of the surfaces used in the dosing lines. This procedure was found to be helpful to minimize the decomposition of NO_2 prior to the admittance to the vacuum chamber. XPS data were acquired with a dual anode, multichannel electrostatic hemispherical analyzer (Omicron, EA-125), using an Al Kα X-ray source ($h\nu$ = 1486.6 eV) and 50 eV pass energy. The X-ray source was oriented ~50° with respect to the sample normal. XPS data were analyzed by fitting the minimum number of Gaussian peaks possible to the experimental spectra. Typical full width at half-maximum values of 2.45−2.50 eV for N 1s features and 2.50−2.55 eV for O 1s features were used, and the resulting residual curves had a total integrated intensity of ≤3% of the corresponding experimental counterparts. Experimental XPS data were calibrated so that the Al $2p^0$ metallic feature of the NiAl(100) substrate was centered at 72.6 eV. NO_2 gas used in the experiments was further purified by several freeze−pump−thaw cycles.

Ultrathin θ-Al_2O_3 films on NiAl(100) were grown by adopting a procedure that was originally suggested by Ibach and co-workers[27,28] which included saturation of the clean NiAl-(100) surface with O_2 at 300 K (total O_2 exposure = 9000 L; 1 L = 1 × 10^{-6} Torr·s^{-1}) and successive oxidation of the O-saturated surface at 1200 K in UHV for 30−60 min to improve the crystallanity of the oxide film.[29−32] The quality of the θ-Al_2O_3 films was checked with AES, XPS, and LEED.[29] The typical film thickness was 6 ± 2 Å.[29]

3. Results and Discussion

3.1. TPD Studies on NO_2/θ-Al_2O_3/NiAl(100). TPD technique was employed to investigate the desorption products that are observed for NO_2 adsorption on a clean θ-Al_2O_3/NiAl(100) surface at 80 K with varying amounts of initial NO_2 exposures. Figure 1 presents such a series of TPD curves corresponding to increasing coverages of NO_2 on the ordered θ-Al_2O_3 film. The most striking characteristic of the TPD spectra given in Figure 1 is that all of the desorption maxima appear at temperatures less than 180 K. This can be more readily seen by examining the inset of Figure 1 emphasizing the TPD data corresponding to T > 180 K. For the lowest dose there is a single desorption maximum at 156 K. The peak value shifts to lower temperatures (from 156 to 133 K) with increasing NO_2 coverage. With further NO_2 coverage increase, a second desorption maximum is seen which becomes the dominant desorption feature at higher coverages with a peak value of 127 K. It is worth mentioning that the line shapes of the TPD data given in Figure 1 for NO_2 adsorption on the θ-Al_2O_3/NiAl(100) surface for T < 200 K closely resemble those of H_2O adsorption on the same surface; the latter was used as a probe molecule to investigate the defect density of the θ-Al_2O_3/NiAl(100) system in our previous study.[29] For the H_2O/θ-Al_2O_3/NiAl(100) system we found that the concentration of surface defects on the θ-Al_2O_3 film lies between 0.05 and 0.10 ML (ML = monolayer).[33] A more detailed analysis regarding the consequences of the similarity between the NO_2 and H_2O TPD line shapes will be given in section 3.3.

Besides NO_2 (i.e., 46 amu) other possible desorption products were also simultaneously monitored, e.g., O_2 (32 amu), N_2 (28 amu), N_2O (44 amu), NO (30 amu), and fragments of N_2O and NO_2. Among these signals, only 30 amu yielded desorption features with intensities higher than the background levels (Figure 2). For T < 180 K, the locations of the 30 amu desorption maxima and line shapes are identical to those for 46 amu (Figure 1) and the absolute 30 amu intensities are higher. It is well-known that NO_2 fragments into lower mass components during its ionization in the QMS, and 30 amu (NO) is dominant. Therefore, the relative intensities of the 46 and 30 amu signals as well as the similarity between the line shapes clearly indicate that the desorption features observed for T < 180 K in Figure 2 are predominantly due to the fragmentation of NO_2 in the QMS (a fraction of the NO desorption signal at T < 180 K can be associated with some disproportionation events that will be discussed in detail in section 3.3).

An important aspect of the 30 amu TPD results is shown in the inset of Figure 2. Unlike the 46 amu signal given in Figure 1, there is a significant 30 amu signal for T > 180 K and the

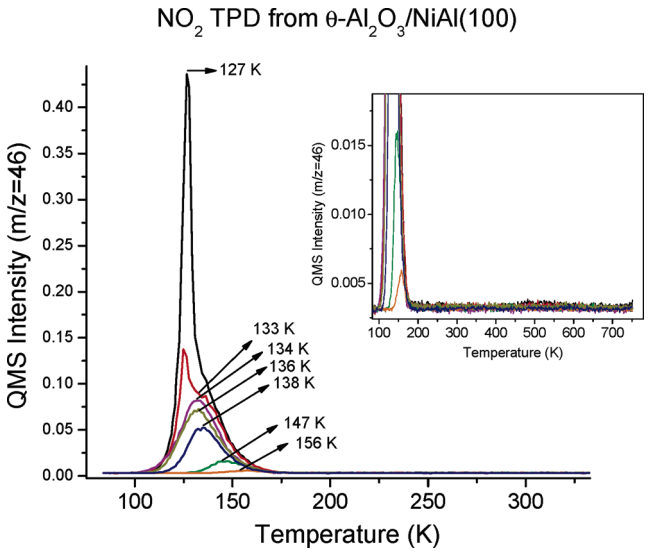

Figure 1. TPD spectra showing the 46 amu (NO_2) desorption signal obtained after adsorption of various doses of NO_2 on clean θ-Al_2O_3/NiAl(100) model catalyst surface. All NO_2 exposures were performed at a surface temperature of 80 K. The inset highlights the elevated temperature region of the TPD curves.

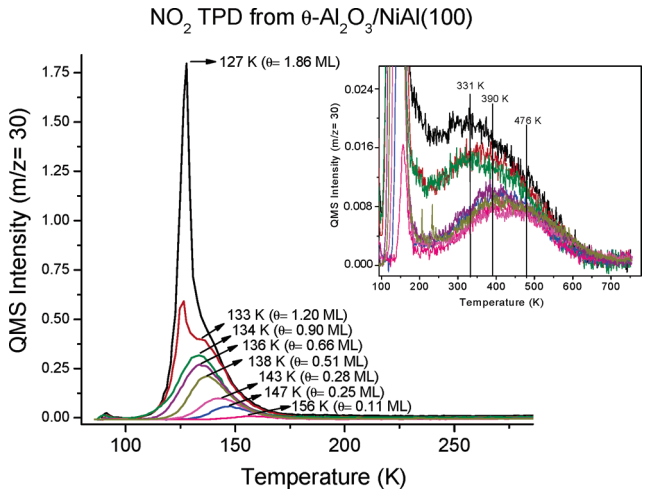

Figure 2. TPD spectra showing the 30 amu desorption signal obtained after adsorption of various doses of NO_2 on clean θ-Al_2O_3/NiAl(100) model catalyst surface. All NO_2 exposures were performed at a surface temperature of 80 K. Note that these series of spectra were obtained simultaneously with the 46 amu signal presented in Figure 1. The inset highlights the elevated temperature region of the TPD curves.

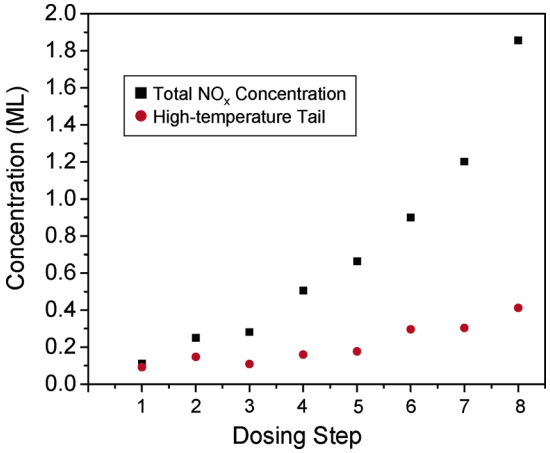

Figure 3. Total NO_x coverage on θ-Al_2O_3/NiAl(100) surface and coverage of NO_x species associated with the high-temperature tail of TPD curves given in Figure 2, as a function of NO_2 dosing steps. Note that dosing steps do not correspond to equal increments in total NO_2 exposures.

intensity increases with the NO_2 exposure. As neither the 46 amu nor the 44 amu signal is detected at $T > 180$ K, the desorption above 180 K is assigned to NO(g). Having assigned desorption products, a more quantitative discussion of the data shown in Figures 1 and 2 is possible. In these spectra, the desorption maximum between 133 and 156 K is attributed to the formation and subsequent saturation of the first NO_2 adsorption layer. The second desorption maximum at 127 K for higher NO_2 exposures is assigned to NO_2 multilayers. Based on this reasoning, the total integrated peak area below the TPD features for the 30 amu signal can be converted to the coverage values shown in Figure 2. The shift of the desorption maxima to lower temperatures with increasing NO_2 coverage in the first monolayer can be ascribed to a perturbed first-order desorption behavior suggesting a repulsive interaction between the NO_2 molecules in the first monolayer. This phenomenon is similar to that observed for H_2O overlayers on the θ-Al_2O_3/NiAl(100) system, where H_2O molecules were suggested to occupy cationic (Al^{3+}) sites that are aligned parallel to the (010) direction on the θ-Al_2O_3 film.[29] The behavior of the desorption maxima at 127 K, corresponding to the multilayer NO_2 adsorption states, is consistent with zero-order desorption also observed for H_2O multilayer desorption. Excluding the strongly bound NO_x species observed as a high-temperature tail in Figure 2 and by only focusing on the global maxima in the TPD curves, it can be argued that the majority of the NO_x, formed upon NO_2 adsorption on θ-Al_2O_3/NiAl(100), binds less strongly than H_2O. The desorption maxima for the monolayer and multilayer adsorption states of H_2O are located at higher temperatures than that for NO_2 ($T_{H_2O,monolayer} = 165$ K, $T_{H_2O,multilayer} = 147$ K vs $T_{NO_2,monolayer} = 134$ K, $T_{NO_2,multilayer} = 127$ K).

Figure 3 provides quantitative information about the relative concentration of the strongly bound NO_x species observed as a high-temperature tail in the TPD spectra given in Figure 2 in comparison with the total NO_x concentration on the θ-Al_2O_3/NiAl(100) surface. Figure 3 shows that, during the initial stages of NO_2 adsorption, strongly bound NO_x states are the major contributors to the total NO_x coverage, whereas with increasing NO_2 exposure their relative contribution settles to about 20% of the total NO_x coverage. It should be noted that the strongly bound NO_x states can reach coverage values of as high as 0.4 ML for a total NO_x coverage of 1.9 ML. Considering the results of previous studies,[29] suggesting a defect concentration of 0.05−0.10 ML for the θ-Al_2O_3/NiAl(100) surface, formation of the strongly bound NO_x species seen in Figure 2 cannot be solely due to the presence of oxygen vacancies or point defect sites.

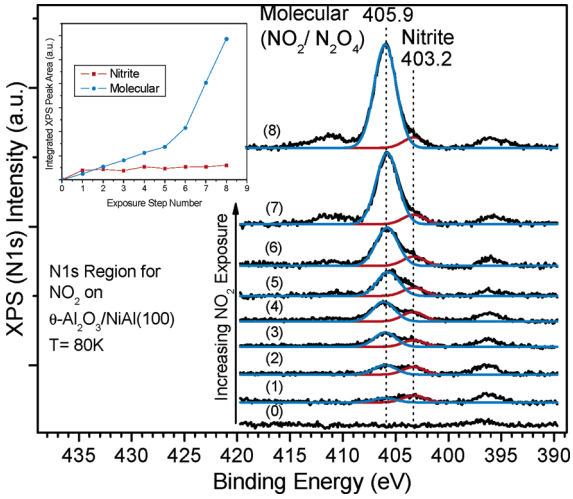

Figure 4. XPS data corresponding to evolution of the N 1s region as a function of NO_2 exposure on clean θ-Al_2O_3/NiAl(100) surface at 80 K. Spectrum (0) represents the clean surface, whereas spectrum (8) corresponds to a NO_2 multilayer ($\theta_{NO_2} \geq 2$ ML). Note that dosing steps do not correspond to equal increments in total NO_2 exposures.

For comparison, after NO exposure at 80 K no detectable amounts of NO desorption were observed, under the exposure regime that was studied (≤50 L), indicating that NO is not stable on the θ-Al_2O_3/NiAl(100) surface at 80 K. We conclude that 30 amu desorption above 180 K in Figure 2 originates from NO species that are formed from NO_2.

3.2. XPS Studies on NO_2/θ-Al_2O_3/NiAl(100). To obtain detailed understanding of the nature of the NO_x species that are formed upon NO_2 adsorption on the θ-Al_2O_3/NiAl(100) model catalyst surface, XPS experiments were performed and changes in the N 1s, O 1s, and Al 2p regions of the X-ray photoelectron spectra were followed to monitor the core level binding energy shifts of the adsorbates as well as the θ-Al_2O_3/NiAl(100) substrate. Figure 4 summarizes the XPS results of the N 1s region corresponding to NO_2 adsorption on the clean and ordered θ-Al_2O_3 film at 80 K with increasing exposures of NO_2. The bottommost spectrum, (0), is for the clean θ-Al_2O_3/NiAl(100) surface, where only a small background feature at ~396 eV is visible. Spectra labeled (1)−(8) are obtained after increasing the total NO_2 exposure in eight steps to reach a total NO_x coverage of $\theta_{NO_x} \geq 2$ ML as shown in the uppermost spectrum, (8). Figure 4 reveals that at low NO_2 exposures, e.g., in spectrum (1), there is a low binding energy (BE) feature centered at 403.2 eV and a smaller intensity feature at 405.9 eV. As the NO_2 exposure is increased, the intensity of the 403.2 eV feature quickly saturates, while the intensity of the 405.9 eV feature continues to grow. Relative intensities of these two features after each dosing step are plotted in the inset of Figure 4. The low BE feature (403.2 eV) in Figure 4 can be assigned to an ionic NO_x species, namely surface nitrites (NO_2^-), based on previously reported results of NO_x adsorption on various oxide surfaces.[11−16] Concurrently, the higher BE feature centered at 405.9 eV in Figure 4 can be attributed to NO_2 that is chemisorbed on the surface in a molecular fashion.[11−15] At 80 K, some ionic nitrite species are formed at low NO_2 exposures, but molecularly chemisorbed NO_2 dominates as the coverage increases. The multilayer states are probably in the form of NO_2 dimers or N_2O_4.[11−15] The formation of ionic nitrite species (NO_2^-) on oxide surfaces was investigated in recent computational studies.[9,17] These results suggested that on alkaline earth

metal oxides NO_2^- is stable but is located 2.8−3.1 Å away from the surface[17]). Adsorbed NO_2^- is stabilized by a strong electrostatic interaction with the oxide. It was proposed that the large separation of the nitrite states interacting electrostatically with the surface yields a loss of the directionality of the nitrite−surface bond as the covalent character of the bond disappears. This, in turn, may bring about a high mobility and an enhanced diffusion capacity for NO_2^- on the oxide surface.[17] This finding is particularly important as the enhanced mobility of the nitrite species on oxide surfaces can improve the reactivity of these species where they can act as precursors for further surface reactions. Furthermore, coexistence of molecular and ionic species at 80 K also deserves attention because it has been proposed that cooperative adsorption of ionic (nitrate or nitrite) species with chemisorbed molecular NO_2 states on the neighboring adsorption sites leads to an additional stabilization of the adsorbate overlayer with respect to adsorption of the same species on isolated surface sites.[9] XPS results presented in Figure 4 also clearly show the lack of a 400−402 eV feature that can be attributed to a NO species, consistent with the instability of these species on the θ-Al_2O_3/NiAl(100) surface within 80−750 K.

Besides the two features mentioned above, an additional artifact with a relatively high BE (ca. 411 eV) is also observed in Figure 4 which becomes more visible particularly in spectra (7) and (8). This feature seems to be closely related to the multilayer states of NO_2 on θ-Al_2O_3/NiAl(100) and disappears at lower NO_2 surface coverages, indicating the possibility that it might be a satellite associated with the molecular/multilayer NO_2. Such a high BE NO_x feature was also observed in a previous work where NO_2 adsorption on ZnO(0001)−Zn and polycrystalline ZnO films was investigated;[15] however, no assignment was given. It can be argued that the high BE feature in Figure 4 is associated with a thick multilayer state consisting of a nitrosonium−nitrate ionic pair ($NO^+NO_3^-$)[34] where the N 1s feature originating from the nitrate ion of the ionic pair is further blue shifted in BE due to its close interaction with the countercation (NO^+). Unfortunately, a NO^+-like feature in the 398−402 eV BE region cannot be seen in the spectra given in Figure 4, suggesting that a nitrosonium−nitrate ionic pair may not be responsible for the observed high BE feature. Another alternative assignment for this feature can be a N_2O_4 isomer which differs in its intramolecular bonding from that of the N_2O_4 state observed at 405.9 eV because N_2O_4 can exist in either OON−NOO or OON−ONO configurations. Therefore, additional vibrational spectroscopic and computational efforts are required for a complete account of this high BE N 1s feature originating from NO_2 adsorption on various metal oxide surfaces.

An important observation that can be deduced by a closer investigation of the XPS data presented in Figure 4 is that the formation of surface NO_3^- species, whose characteristic BE is known to be within 407−408.5 eV, is not observed upon NO_2 adsorption on θ-Al_2O_3/NiAl(100) model catalyst surface at 80 K regardless of the NO_2 exposure. This is an interesting observation as the nitrates (NO_3^-) have been proposed to be highly stable NO_x species that are formed upon NO_2 adsorption on a number of metal oxide surfaces including MgO(001), CaO(001), SrO(001), and BaO(001),[9] TiO_2(110),[11] polycrystalline CeO_2 films,[14] Fe_2O_3 powders,[14] CuO powders,[14] ZnO powders,[14] and γ-Al_2O_3 powders.[8,10] Lack of the formation of nitrate species at 80 K implies a thermal activation barrier for the formation of NO_3^- on θ-Al_2O_3/NiAl(100).

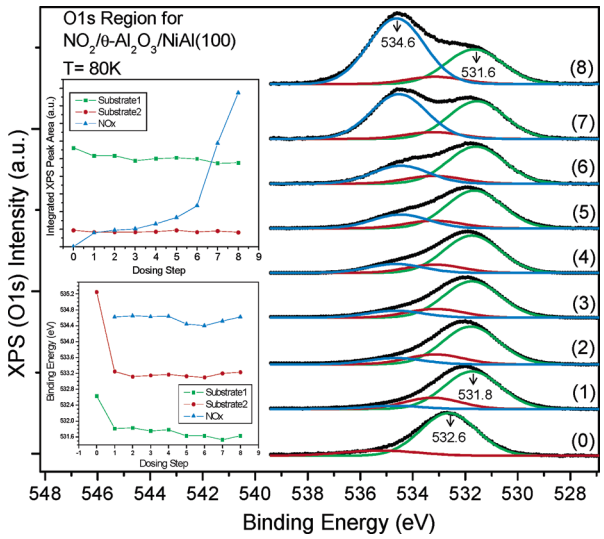

Figure 5. XPS data of the O 1s region as a function of NO_2 exposure on clean θ-Al_2O_3/NiAl(100) surface at 80 K. Spectrum (0) represents the clean surface, whereas spectrum (8) corresponds to a NO_2 multilayer ($\theta_{NO_2} \geq 2$ ML). Relative changes in the BE values and the integrated XPS peak areas for different species are also given in the insets. Note that dosing steps do not correspond to equal increments in total NO_2 exposures.

Figure 5 shows the evolution of the O 1s region of the X-ray photoelectron spectra which is obtained simultaneously with the series of spectra given in Figure 4. Changes in the BE of the substrate and adsorbate O 1s levels as well as the changes in the integrated XPS intensities as a function of dosing steps are also plotted in the upper and lower insets, respectively. The bottommost spectrum, (0), in Figure 5 represents an asymmetric O 1s signal resulting from the clean θ-Al_2O_3/NiAl(100) substrate whose peak position is located at 532.6 eV.[32,35] Spectrum (1) in Figure 4 indicates that, immediately after the introduction of a small dose of NO_2 on the θ-Al_2O_3/NiAl(100) surface, formation of ionic NO_x species (i.e., NO_2^-) is observed. Spectrum (1) in Figure 5 suggests that formation of these ionic species has an observable influence on the O 1s levels of the θ-Al_2O_3 substrate resulting in a red shift of −0.8 eV in the major substrate O 1s feature, implying a strong electrostatic interaction between the nitrite species and the oxide surface. It can be readily seen in Figure 5 that further increase in the NO_2 exposure does not have a significant effect on the substrate O 1s levels except for a slight attenuation of their intensities. This is consistent with the observation that at higher NO_2 exposures molecularly chemisorbed NO_2 states dominate the NO_x population on the surface which interacts covalently with the surface and not electrostatically. The additional O 1s feature that starts to develop with increasing NO_2 exposure can be readily attributed to the nitrite and chemisorbed molecular NO_2 states. These O 1s signals in the XPS yield a broad feature located at a BE of 534.6 eV.

The effect of the surface temperature on the NO_2 adsorption on θ-Al_2O_3/NiAl(100) was examined using XPS. The results, given in Figure 6, correspond to an NO_2 multilayer ($\theta_{NO_2} \geq 2$ ML) that is adsorbed on a clean θ-Al_2O_3/NiAl(100) surface at 80 K. After the initial deposition of a NO_2 multilayer, the surface was flashed up to the given temperatures, and cooled back to 80 K before the XPS data were acquired. Changes in the relative BE values as well as the integrated XPS areas were also plotted in the insets in Figure 6. The uppermost spectrum of Figure 6 corresponding to 80 K yields a typical XPS spectrum for a NO_2 multilayer on θ-Al_2O_3/NiAl(100). Increasing the surface tem-

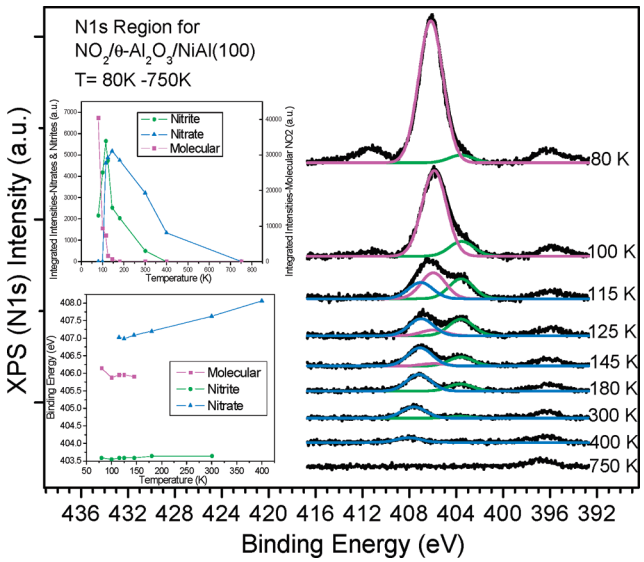

Figure 6. XPS data of the N 1s region after adsorption of a NO_2 multilayer ($\theta_{NO_2} \geq 2$ ML) at 80 K on θ-Al_2O_3/NiAl(100) and subsequent annealing. Relative changes in the BE values and the integrated XPS peak areas for different species are also given in the insets.

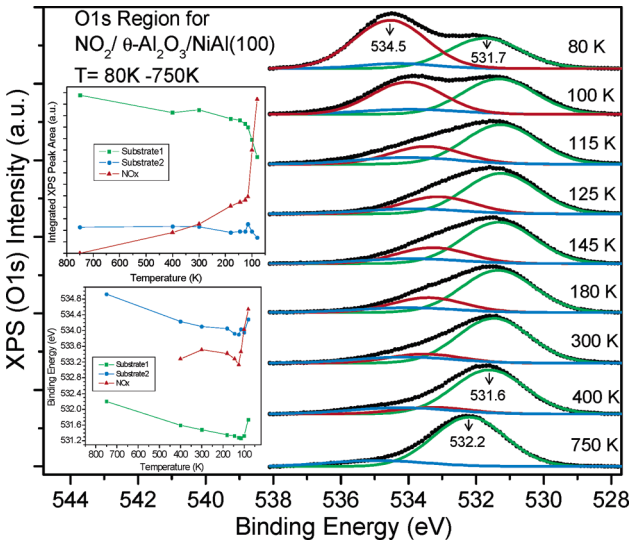

Figure 7. XPS data of the O 1s region after adsorption of a NO_2 multilayer ($\theta_{NO_2} \geq 2$ ML) at 80 K on θ-Al_2O_3/NiAl(100) and subsequent annealing. Relative changes in the BE values and the integrated XPS peak areas for different species are also given in the insets.

perature to 100 K results in some NO_2 desorption from the oxide surface as anticipated from the TPD data given in Figures 1 and 2. This is also evident from the significant decrease in the intensity of the molecular ($NO_2 + N_2O_4$) signal in the XPS data obtained at 100 K. Furthermore, a slight increase in the intensity of the nitrite signal is visible. At 115 K, a further increase in the nitrite concentration is accompanied by a decrease in the surface population of molecular NO_2 states where the concentration of the nitrites reaches its maximum value. The most important aspect of the X-ray photoelectron spectrum at 115 K is the appearance of an additional NO_x feature located at 407.0 eV. Based on the BE position of this feature, it can be assigned to a nitrate (NO_3^-) species.[11−15] At higher temperatures such as 125 K, conversion of molecular NO_2 states into ionic NO_x species continues and the intensity of the nitrate signal continues to increase. At 145 K little of the molecular NO_2 species remains; surface nitrites and nitrates dominate. Furthermore, by comparing the relative intensities of different ionic species, it can be seen that the surface concentration of the nitrates starts to exceed that of the nitrites. With a further increase in the surface temperature to 300 K, the total NO_x coverage drops and only NO_3^- species remain. At 400 K, nitrate coverage attenuates, and at 750 K all of the NO_x species are removed, consistent with the TPD data given in Figures 1 and 2.

As expected, changes in the core level shifts of the O 1s region upon annealing (Figure 7) are reversed compared to adsorption (Figure 5). A broad and an intense O 1s feature originating from the molecular NO_2 and N_2O_4 and ionic NO_2^- states is located at 534.5 eV (80 K). The peak shifts to 533.3 eV at low coverages, where the surface is dominated by ionic nitrate species ($T \geq 300$ K). After complete desorption of NO_x (750 K), the O 1s signal returns to 532.2 eV.

High-pressure ex situ NO_2 adsorption experiments were also performed on the θ-Al_2O_3/NiAl(100) model catalyst surface to mimic a more realistic catalytic environment and investigate the stability of the NO_x species formed on the model catalyst surface under elevated temperature and pressure conditions. Figure 8 compares N 1s XPS results before and after exposing a θ-Al_2O_3 film to 1.5 Torr of NO_2 at 300 K (total NO_2 exposure of 4.5×10^8 L and subsequent evacuation at 300 K). Consistent with the above UHV results, nitrates (NO_3^-) are the only stable

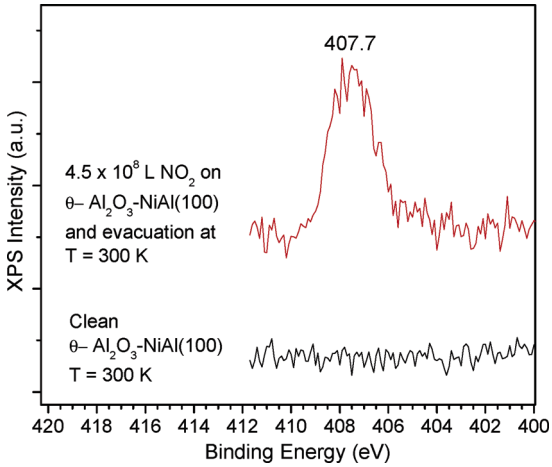

Figure 8. Ex situ XPS results obtained after exposing clean θ-Al_2O_3/NiAl(100) model catalyst surface to NO_2 pressure of 1.5 Torr at 300 K and subsequent evacuation at the same temperature.

NO_x species observed upon high-pressure NO_2 exposure and evacuation at 300 K.

Figure 9 focuses on the effect of the NO_x adsorption states on the Al 2p levels of the θ-Al_2O_3/NiAl(100) system at various temperatures. The series of spectra given in Figure 9 corresponds to a multilayer of NO_2 adsorbed on the alumina film as in the case of Figures 4−7. The uppermost spectrum in Figure 9 represents the clean θ-Al_2O_3 film obtained after desorbing all the NO_x species from the surface. The spectrum acquired at 400 K shows that even the presence of a small concentration of ionic NO_x species on the surface (in this case NO_3^-) strongly influences the Al^{3+} and $Al^{(3-x)+}$ 2p core levels of the oxide which is reflected in the −0.6 eV red shift of the Al^{3+} and $Al^{(3-x)+}$ 2p peak maximum. The strong influence of the ionic NO_x species on the cationic core levels continues to be visible until 145 K. The effect of the increasing surface NO_x coverage (mostly due to molecularly chemisorbed NO_2 states) only attenuates the intensity of the Al^{3+} and $Al^{(3-x)+}$ 2p signal without a further significant chemical shift. Molecular NO_2 does not alter the Al $2p^0$ metallic core levels of the NiAl(100) substrate. The behavior of the Al 2p region of the X-ray photoelectron spectra for various doses of NO_2 at 80 K (not shown) exhibited

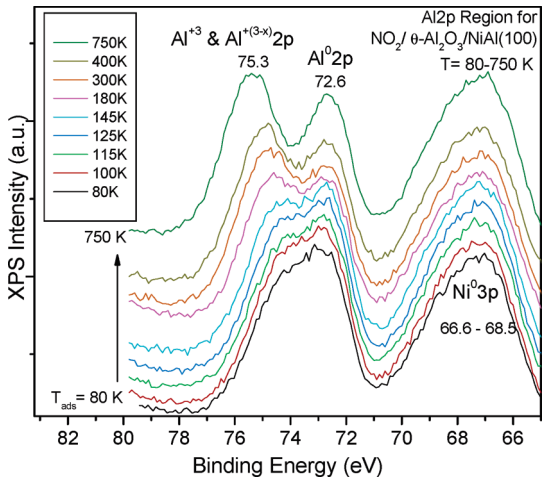

Figure 9. XPS data of the Al 2p region after multilayer ($\theta_{NO_2} \geq 2$ ML) adsorption of a NO_2 at 80 K on θ-Al_2O_3/NiAl(100) and subsequent annealing.

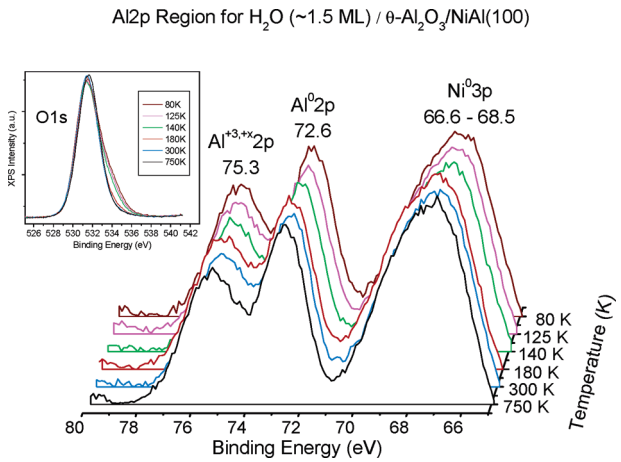

Figure 10. XPS data of the Al 2p region after adsorption of a H_2O multilayer ($\theta_{H_2O} \sim 1.5$ ML) at 80 K on θ-Al_2O_3/NiAl(100) and subsequent annealing.

general trends similar to those of Figure 9 except nitrites rather than nitrates were observed in N 1s XPS.

For comparison, Figure 10 presents XPS results of analogous experiments using H_2O, which is known to adsorb exclusively in a molecular fashion.[29,33] Due to the lack of a strong electrostatic interaction between the H_2O overlayer and the alumina surface, Al^{3+} and $Al^{(3-x)+}$ 2p signal of the oxide film is barely affected upon H_2O adsorption, although molecular adsorption modes of H_2O have stronger binding on the θ-Al_2O_3/NiAl(100) surface in the mono- and multilayer states with respect to that of NO_2.

3.3. Chemistry of NO_2 on θ-Al_2O_3/NiAl(100). The interaction of NO_2 with the θ-Al_2O_3/NiAl(100) model catalyst surface can be analyzed in more detail in the light of the TPD and XPS results presented in the previous sections.

TPD and XPS results confirm that adsorption of NO_2 in the monolayer and the subsequent multilayers at $T < 115$ K is mostly molecular without a significant contribution from either dissociative adsorption or disproportionation. XPS data reveal the presence of molecular NO_2 states and nitrites at 80 K (Figure 3), while the formation of NO(ads) or NO_3^-(ads) states was not observed. In addition, considering the similarity of the TPD line shapes corresponding to NO_2 adsorption with respect to that of H_2O adsorption on the alumina film, where H_2O was suggested to occupy Al^{3+} cation sites,[29] it can be argued that in the first monolayer NO_2 occupies cationic (Al^{3+}) sites. Considering the θ-Al_2O_3 film structure,[27,28] NO_2 probably adsorbs in a bridging geometry such that the O atoms of NO_2 are directed toward two neighboring cation sites. Such an orientation in which NO_2 binds to two cation sites through its O atoms, rather than sitting on an anion site in a monodentate fashion, was proposed to be energetically more favorable for NO_2 adsorption on TiO_2(110) surface.[11] This proposed orientation is consistent with a repulsive interaction, that leads to a perturbed first order desorption kinetics in the monolayer regime (TPD data of Figures 1 and 2). The repulsion arises between NO_2 molecules aligned along the cation rows[29] of the oxide surface.

The relative stability of the NO_x species that are formed upon NO_2 adsorption on the θ-Al_2O_3/NiAl(100) model catalyst surface can also be discussed using the data given in Figures 1−8. XPS and TPD data reveal that multilayer NO_2 (i.e., molecular NO_2 and probably N_2O_4) is stable up to ca. 125 K. Chemisorbed NO_2 in the monolayer is still stable up to 145 K, while ionic species, i.e., nitrites and nitrates, are significantly more stable. They are readily detectable by XPS (Figure 6) at temperatures as high as 300 and 400 K, respectively. TPD data (Figure 2) also suggest that complete desorption of the stable ionic species requires a surface temperature of 650 K. Therefore, under the conditions where NO_3^- formation is not limited by kinetics, relative stabilities of the NO_x species existing on the θ-Al_2O_3/NiAl(100) surface can be ranked in the order of increasing stability as follows: NO_2(physisorbed or N_2O_4) < NO_2 (chemisorbed) < NO_2^- < NO_3^-.

Figures 4 and 6 imply that nitrites can easily form on the θ-Al_2O_3/NiAl(100) surface even at 80 K and are stable up to 300 K. A recent computational study[17] suggests that electron-transfer events from an alkaline earth metal oxide to NO_2 molecules are significantly facilitated on the steps and corners of the oxide surface. It is known from scanning tunneling microscopy (STM) studies[30−32] that θ-Al_2O_3/NiAl(100) films exhibit a stepped morphology. These steps and corners likely facilitate electron transfer from the oxide to NO_2 and are responsible for nitrite formation at temperatures as low as 80 K.

The formation of nitrates is also an interesting point to discuss in detail. Although nitrates as noted above are the most stable NO_x species on the θ-Al_2O_3/NiAl(100) surface, they are not observed at $T < 115$ K. It should be noted that, for $T < 115$ K, a covalent interaction between the N atom of the adsorbed NO_2 molecules with the anionic (O^{2-}) sites of the surface leading to a NO_3^--like species as shown in the following reaction

$$NO_2(g) + O(\text{lattice}) \rightarrow NO_3(\text{ads}) \quad (1)$$

is not evident in the XPS results (Figures 4 and 6). Evidently, NO_3^- formation requires thermal activation.

Various mechanistic pathways for the nitrate formation that include a thermally activated bond scission process can be considered. One possible mechanism for the formation of nitrates is dissociation of NO_2(g) to yield NO(g) and surface O(ads) followed by the reaction between O(ads) and NO_2(g) as given in reactions 2 and 3:

$$NO_2(g) \rightarrow NO(g) + O(\text{ads}) \quad (2)$$

$$NO_2(g) + O(\text{ads}) \rightarrow NO_3(\text{ads}) \quad (3)$$

Because reaction 2 in this mechanistic pathway is an endothermic process ($NO_2(g) \rightarrow NO(g) + O(g)$, $\Delta H = 73$ kcal/mol[14]),

NO_2 dissociation followed by the reaction of resulting atomic O and surface NO_2 is consistent with the formation of nitrates at $T > 115$ K but not at 80 K.

Similar observations regarding the temperature dependence of nitrate formation was recently reported for NO_2 adsorption on a TiO_2(110) surface[11] where, despite their high stability, nitrates were not observed at low temperatures. The experimental data and computational results[11] suggested that nitrate formation involved a disproportionation mechanism:

$$2NO_2(ads) \rightarrow NO_3(ads) + NO(g) \quad (4)$$

This mechanism is also consistent with the current XPS results shown in Figure 6 which indicate that chemisorbed NO_2 and ionic nitrite states precede the formation of surface nitrates.

It should also be noted that both of these thermally activated mechanistic pathways for nitrate formation may not be solely limited to the cationic sites on the terraces of the oxide surface, but are likely to occur on the oxygen vacancies as well. The concentration of these point defects is within 0.05−0.10 ML,[29,33] well below the maximum coverage of ionic NO_x species (0.4 ML in Figure 3). Thus, the total concentration of point defects is not high enough to account for all of the nitrate formation, and the nitrate formation events should be occurring on point defects as well as on regular terrace cationic sites (Al^{3+}), and/or extended defects.[33]

TPD results shown in Figures 1 and 2 illustrate that the strongly bound ionic nitrate and nitrite species desorb to yield NO(g) between 180 and 650 K. In addition, as was mentioned earlier, the 32 amu signal (monitored simultaneously with the 30 and 46 amu signals in the TPD) was completely absent. This suggests that during desorption/decomposition of nitrate and nitrite species, O_2 was not formed as would be expected from reactions 2, 5, and 6:

$$NO_3(ads) \rightarrow NO_2(ads) + O(ads) \quad (5)$$

$$O(ads) + O(ads) \rightarrow O_2(g) \quad (6)$$

Several mechanisms may determine the fate of the O atoms formed via reactions 2 and 5. Some O atoms are likely to diffuse on the surface to fill O vacancies (point defects). In a similar way, some O atoms may also decorate extended defect sites such as steps[38] and atomic oxygen can also diffuse into the subsurface region or into the θ-Al_2O_3/NiAl(100) interface. An alternative possibility based on a recent computational study[11] suggested that NO_2 adsorption on TiO_2(110) can result in the diffusion of oxygen vacancies from the bulk/subsurface region to the oxide surface. In the current study, we also performed LEED experiments to investigate the degree of surface order after NO_2 adsorption and subsequent desorption from the θ-Al_2O_3/NiAl(100) surface. The results of these experiments indicated that, although the primary and half-order spots corresponding to a θ-Al_2O_3 structure were still clearly visible after the adsorption/desorption experiments, LEED images of the alumina films obtained after the adsorption/desorption experiments consisted of relatively diffuse diffraction spots, suggesting some loss of long-range ordering. These postreaction LEED experiments are consistent with a surface roughening and/or partial reconstruction of the alumina surface structure.[39,32] Taken together, the results suggest that O atoms produced upon decomposition of ionic NO_x species on the θ-Al_2O_3/NiAl(100) surface do not desorb from the surface via a recombinative coupling process (reaction 6); rather they lead to structural transformations in the film morphology (decoration of point defects and extended defects of the oxide surface by the O atoms and O diffusion to the subsurface).

The adsorption and reaction of NO_2 on the θ-Al_2O_3/NiAl(100) model catalyst surface (Figures 5, 7, and 9) clearly influences the core levels of the θ-Al_2O_3 film but not the Al 2p features associated with the NiAl(100) bimetallic substrate. The most interesting aspect of the adsorbate induced core level shifts of the oxide film given in Figure 9 (as well as the Al 2p region of the XPS results obtained for NO_2 adsorption experiments at various coverages at 80 K that are not shown here) appears at low total NO_x coverages (750−180 K). It is apparent that under these coverage conditions ($\theta_{NO_x} < 0.5$ ML), NO_x states are dominated by strongly bound ionic species, and Al^{3+} and $Al^{(3-x)+}$ 2p features of the oxide film exhibit a red shift in BE whose magnitude increases with increasing coverage. Upon saturation of the ionic NO_x species the surface starts to be populated by less strongly bound molecular NO_2 states, and the red shift in the Al^{3+} and $Al^{(3-x)+}$ 2p oxide features also stabilizes. The BE shifts associated with the Al^{3+} sites of the oxide film are accompanied by similar BE shifts in the O 1s levels of the anion sites of the oxide film as seen in Figures 5 and 7. These BE shifts induced by ionic NO_x species in the Al 2p and O 1s regions are similar in direction (i.e., a red shift) as well as magnitude ($\Delta E_{BE} \leq 0.8$ eV). Adsorbate induced BE shifts that are consistent with the observations presented in the current work have also been reported in NO_2 adsorption on a TiO_2(110) surface,[11] where a BE shift of −0.5 eV was observed for the O 1s levels of the oxide surface and were attributed to adsorbate induced band bending.[11,40,41] Our results indicate that the magnitude of the induced BE shifts is related to the nature and/or the strength of the bonding between the adsorbate and the oxide surface. This is demonstrated in Figure 10, where the interaction of weakly bound probe molecule (H_2O) and the θ-Al_2O_3/NiAl(100) surface does not significantly alter the Al^{3+} and $Al^{(3-x)+}$ 2p binding energy of the oxide features.

4. Conclusions

In this paper, TPD and XPS techniques were employed to investigate the fundamental aspects of the interaction between NO_2 and a θ-Al_2O_3/NiAl(100) model catalyst surface. Our findings can be summarized as follows:

(a) The main conclusion of the current report is that alumina support is not completely inert in NO_x storage systems and may stabilize some NO_x species under certain catalytic conditions. The origin of the NO_x uptake of the catalyst support (i.e., Al_2O_3) in NO_x storage materials should be associated with the conversion of adsorbed NO_2 to nitrates and nitrites that are stable on alumina at temperatures as high as 650 K.

(b) At 80 K the formation of only molecularly chemisorbed NO_2 states and nitrite species was observed.

(c) Temperature-dependent experiments reveal that, at $T >$ 180 K, nitrate formation can also occur on the θ-Al_2O_3 surface in addition to NO_2^- and chemisorbed NO_2. Relative stability of the NO_x species observed on the θ-Al_2O_3 model catalyst upon NO_2 adsorption can be ranked with increasing stability as NO_2 (physisorbed or N_2O_4) < NO_2 (chemisorbed) < NO_2^- < NO_3^-.

Acknowledgment. We gratefully acknowledge the US Department of Energy (DOE), Office of Basic Energy Sciences, Division of Chemical Sciences, for the support of this work. The research described in this paper was performed at the Environmental Molecular Sciences Laboratory (EMSL), a national scientific user facility sponsored by the DOE Office of Biological and Environmental Research and located at Pacific

Northwest National Laboratory (PNNL). PNNL is operated for the US DOE by Battelle Memorial Institute under Contract No. DE-AC05-76RL01830. The authors would like to acknowledge with pleasure Drs. Mark H. Engelhard, Zdenek Dohnálek, Michael A. Henderson, J. Mike White, D. Wayne Goodman, Ja Hun Kwak, Tamás Szailer, Do Heui Kim, William F. Schneider, and Jose E. HerreraPerea for fruitful discussions.

References and Notes

(1) Henrich, V. E.; Cox, P. A. *The Surface Science of Metal Oxides*; Cambridge University Press: Cambridge, 1994.

(2) Taylor, K. C. *Catal. Rev.—Sci. Eng.* **1993**, *35*, 457.

(3) Shelef, M. *Chem. Rev.* **1995**, *95*, 209.

(4) Ozensoy, E.; Goodman, D. W. *Phys. Chem. Chem. Phys.* **2004**, *6*, 3765.

(5) Takeuchi, M.; Matsumoto, S. *Top. Catal.* **2004**, *28*, 151.

(6) Gill, L. J.; Blakeman, P. G.; Twigg, M. V.; Walker, A. P. *Top. Catal.* **2004**, *28*, 157.

(7) Burch, R. *Catal. Rev.* **2004**, *46*, 271.

(8) Westerberg, B.; Fridell, E. *J. Mol. Catal. A* **2001**, *165*, 249.

(9) Schneider, W. F. *J. Phys. Chem. B* **2004**, *108*, 273.

(10) Paze, C.; Gubitosa, G.; Giacone, S. O.; Spoto, G.; Xamena, F. X. L. I.; Zecchina, A. *Top. Catal.* **2004**, *30*−*31*, 169.

(11) Rodriguez, J. A.; Jirsak, T.; Liu, G.; Hrbek, J.; Dvorak, J.; Maiti, A. *J. Am. Chem. Soc.* **2001**, *123*, 9597.

(12) Rodriguez, J. A.; Perez, M.; Jirsak, T.; Gonzalez, L.; Maiti, A.; Larese, J. Z. *J. Phys. Chem. B* **2001**, *105*, 5497.

(13) Rodriguez, J. A.; Jirsak, T.; Kim, J. Y.; Larese, J. Z.; Maiti, A. *Chem. Phys. Lett.* **2000**, *330*, 475.

(14) Rodriguez, J. A.; Jirsak, T.; Sambasivan, S.; Fischer, D.; Maiti, A. *J. Chem. Phys.* **2000**, *112*, 9929.

(15) Rodriguez, J. A.; Jirsak, T.; Chaturvedi, S.; Dvorak, J. *J. Mol. Catal. A* **2001**, *167*, 47.

(16) Schmitz, P. J.; Baird, R. J. *J. Phys. Chem. B* **2002**, *106*, 4172.

(17) Branda, M. M.; Di Valentin, C.; Pacchioni, G. *J. Phys. Chem. B* **2004**, *108*, 4752.

(18) Karlsen, E. J.; Nygren, M. A.; Petterson, L. G. M. *J. Phys. Chem. B* **2003**, *107*, 7795.

(19) Torres, J.; Perry, C. C.; Bransfield, S. J.; Fairbrother, D. H. *J. Phys. Chem. B* **2003**, *107*, 5558.

(20) Hess, C.; Lunsford, J. H. *J. Phys. Chem. B* **2003**, *107*, 1982.

(21) Broqvist, P.; Grolnbeck, H.; Fridell, E. *J. Phys. Chem. B* **2004**, *108*, 3523.

(22) Szanyi, J.; Kwak, J. H.; Kim, D. H.; Burton, S. D.; Peden, C. H. F. *J. Phys. Chem. B* **2005**, *109*, 27.

(23) Fridell, E.; Skoglundh, M.; Westerberg, B.; Johansson, S.; Smedler, G. *J. Catal.* **1999**, *183*, 196.

(24) Prinetto, F.; Ghiotti, G.; Nova, I.; Lietti, L.; Tronconi, E.; Forzatti, P. *J. Phys. Chem. B* **2001**, *105*, 12732.

(25) Stone, P.; Ishii, M.; Bowker, M. *Surf. Sci.* **2003**, *537*, 179.

(26) Di Valentin, C.; Figini, A.; Pacchioni, G. *Surf. Sci.* **2004**, *556*, 145.

(27) Gassmann, P.; Franchy, R.; Ibach, H. *Surf. Sci.* **1994**, *319*, 95.

(28) Gassmann, P.; Franchy, R.; Ibach, H. *J. Electron Spectrosc. Relat. Phenom.* **1993**, *64*/*65*, 315.

(29) Ozensoy, E.; Szanyi, J.; Peden, C. H. F. *J. Phys. Chem. B* **2005**, *109*, 3431.

(30) Fremy, N.; Maurice, V.; Marcus, P. *J. Am. Ceram. Soc.* **2003**, *86*, 669.

(31) Fremy, N.; Maurice, V.; Marcus, P. *Surf. Interface Anal.* **2002**, *34*, 519.

(32) Maurice, V.; Fremy, N.; Marcus, P. *Surf. Sci.* **2005**, *581*, 88.

(33) Previous STM studies (refs 30−32) suggest that θ-Al_2O_3 films grown on NiAl(100) substrates exhibit extended defects such as edges and line defects. Therefore, we believe that the relatively small value (ref 29) of the surface defect density estimated via H_2O adsorption on the θ-Al_2O_3 films under low-exposure/low-temperature conditions (<5 L, $T_{ads} = 80$ K) is associated with the dissociation of H_2O on the oxygen vacancies or other point defects in the terraces of the oxide surface. In other words, extended defects such as steps seem to be inactive in H_2O dissociation under the low-exposure regime and the low initial adsorption temperatures that were investigated in ref 29. It should be noted that a recent STM study (ref 32) indicates that H_2O adsorption at higher pressures (10^{-7}−10^{-5} Torr) and exposures (60−3000 L) performed at elevated surface temperatures such as 300 K leads to hydroxylation and reconstruction of the alumina surface.

(34) Jones, L. H.; Swanson, B. I.; Agnew, S. F. *J. Chem. Phys.* **1985**, *82*, 4389.

(35) Such a shoulder toward the high BE side was also typically observed for γ-Al_2O_3 ultrathin films grown on NiAl(110) bimetallic substrates (see, for example, refs 36 and 37).

(36) Tzvetkov, G.; Zubavichus, Y.; Koller, G.; Schmidt, Th.; Heske, C.; Umbach, E.; Grunze, M.; Ramsey, M. G.; Netzer, F. P. *Surf. Sci.* **2003**, *543*, 131.

(37) Libuda, J.; Frank, M.; Sandell, A.; Andersson, S.; Bruhwiler, P. A.; Baumer, M.; Martensson, N.; Freund, H. J. *Surf. Sci.* **1997**, *384*, 106.

(38) Kolmakov, A.; Stultz, J.; Goodman, D. W. *J. Chem. Phys.* **2000**, *113*, 7564.

(39) Schauermann, S.; Johanek, V.; Laurin, M.; Libuda, J.; Freund, H. J. *Chem. Phys. Lett.* **2003**, *381*, 298.

(40) Wu, Y.; Garfunkel, E.; Madey, T. E. *Surf. Sci.* **1996**, *365*, 337.

(41) Hu, J.; Pan, J.; Zhu, F.; Gong, H. *J. Appl. Phys.* **2004**, *95*, 6273.